LOCAL REPAIR OF PRECAST CONCRETE BEAMS USING BONDED COMPOSITE PATCH

Ozgur Yapar, Vanderbilt University, Nashville, TN
P.K. Basu, D.Sc., PE, Vanderbilt University, Nashville, TN
Wayne Seger, PE, Tennessee Department of Transportation, Nashville, TN
Jacob N. McNutt, Vanderbilt University, Nashville, TN
Nikolas A. Nordendale, Vanderbilt University, Nashville, TN

ABSTRACT

Extending the life of bridge structures through bonded patch repair of localized damages is an attractive option because of improved structural performance and ease of undertaking certain types of repair rapidly. This paper is based on the research work recently undertaken at Vanderbilt University with funding support from Tennessee Department of Transportation. Apart from investigating various options for patch repair, both analytical and experimental investigations were undertaken. In the analytical treatment a mechanistic model was developed to predict the outcome of patch repair which was further verified through finite element modeling. In addition, simple mechanics based formulas were developed for preliminary design of the patch. Model prestressed precast beams were manufactured and tested in the laboratory to verify the performance of the repair. Finally, analytical and experimental results of the study were compared and some interesting conclusions were drawn.

Keywords: Bridge, Life-Extension, Precast, Bonded, FRP, Patch

INTRODUCTION

Nearly one-third of about 0.6 million bridges in our nation's transportation infrastructure are either structurally deficient, functionally obsolete, or both. The estimated price tag for replacing all the deficient and/or obsolete bridges within a few years is about $140 billion, Schust[1]. A sizeable percentage (about 30%) of all the bridges has precast concrete girders. Majority of these bridges were built in the 20th century and were designed to last 50 years or more. The age of a large proportion of these bridges is 40 years or more, and is undergoing deterioration as a result of chloride-ion penetration, carbonation, alkali-silicate reaction, sulfate attack, leaching and freeze-thaw and thermal cycles hastened by the corrosion of the embedded steel reinforcements and strands. Construction and design errors may also have contributed to the process. The aging process of a bridge may be accelerated by abnormally heavier, larger, and faster traffic loads. A very common form of damage caused to the soffit of bridge girders is by the impact of over-height vehicles in violation of warning signs on actual vertical clearance. In Fig. 1 is shown the bottom of girder damaged by vehicle impact exposing some of the strands.

Fig. 1 Exposed strands due to damage caused by truck impact (Harries et al.[2])

Inadequacy of available financial resources does not allow quick replacement or retrofitting of deficient and/or obsolete bridges and effective, low-cost and rapid repair schemes must be adopted to prolong the useful life of the deteriorating bridges. So, apart from timely maintenance and strengthening, repair should be the hallmark of effective management of highway infrastructure, so that an economically feasible long-term replacement or major rehabilitation plan can be put in place. Required methods and procedures to be used for repair will depend upon the nature, location and extent of damage, and the selected repair material, requiring considerations on case-by-case basis. This also calls for developing innovative schemes that are cost effective, cause minimum interference with the traffic, and avoid even a short-term temporary closure of the bridge. The repair or strengthening scheme adopted for a particular bridge should be based on a clear understanding of materials to be

used and methods to be followed as well as the resulting effects on short- and long-term structural behavior of the adopted life enhancement scheme. The type of deficiency in the structure addressed here may be local damage, say, in the form of structural cracks (shear and/or flexure), local loss of surface material due to spalls say, caused by vehicle impact, and erosion, or local inadequacy of capacity resulting from errors or mistakes in design and/or construction. In every case it is, however, assumed that, in the presence of deficiency, the structure is capable of supporting normal service load before corrective action and that only the reserve capacity of the structure has been compromised.

Of the many currently available materials with potential for repairing bridge structures, the material of choice in this study is bonded composite patch material, namely, fiber reinforced polymers (FRP). After the first initial trials in Europe (Basu[3] et al.), FRP began its distinct presence in the civil engineering community, beginning in the 1980s, as a viable option for structural repair and post-strengthening. Interest in FRP composite systems rose from the many drawbacks of post-strengthening of structures with conventional materials, especially steel; and continues to be the motivation for investigating FRP composites for conditions in the USA. Such materials are typically comprised of resin matrix embedded with carbon, glass, and, less commonly, aramid fibers. FRP laminates are lightweight and incredibly strong compared with the classic patch materials, namely steel, grout, cement, and concrete; making it ideal for placement. Laminated FRP has been most popular in strengthening concrete members (like columns in a bridge pier) as wrapped-on-jacket over deteriorated concrete. The aerospace industry has been using, for some time, patch repair techniques for the body of aircrafts, initially, with riveted metal patches, but later with bonded laminated composite patches to ensure better fatigue life (Ahn[4] et al.). Likewise, FRP is a candidate for patch repair of localized damages (deteriorations) in precast bridge girders, and, possibly, deck slabs. The potential advantages of laminated fiber reinforced polymers for such repair can be identified as easy and quick installation, savings in labor and shutdown costs, possibility of customization with respect to size, shape, and strength, superior durability, high strength to weight ratios, and lightweight.

In the United States, FRP patch repair is yet to find widespread acceptance in the bridge engineering community due to higher cost of available materials, lack of familiarity with materials and processes, extremely limited availability of such material customized for direct civil engineering applications away from controlled factory environment, and lack of product standardization by the manufacturers, supposedly for incorporation in design and construction standards. It is hoped that in this post-recession era, with politicians calling for budget cuts on all fronts, FRP patch repair will emerge as a workable low-cost approach to extending the life of a sizeable proportion of our deteriorating bridge infrastructure. A precursor to all this is a thorough evaluation of the perceived repair schemes using short- and long-term experimental and analytical studies, covering every stage of the strengthening process, including the effect on fatigue life. Ongoing research efforts at several institutions to investigate the nature and behavior of FRP as patch repair material are a welcome development. In this context, some of the experimental and analytical research work being undertaken at Vanderbilt University on FRP patch repair of precast prestressed concrete beams with the support from Tennessee Department of Transportation is being reported here.

Based on investigation of various fiber and matrix material alternatives in terms of mechanical properties, ease of application, and cost/benefit ratios, the current consensus is in favor of using carbon fiber reinforced polymers (CFRP) for repairing beams, and columns. The failures modes of FRP composite repaired component have been identified as (Meier[5]):

- FRP separation from substrate by peeling
- Delamination within composite plies
- Concrete failing in compression
- Concrete shearing in tensile regions
- Sudden failure of FRP with little warning

Methods to avoid some of these modes have been identified. The structural integrity of such repair due to exposure to freeze-thaw and thermal cycles has also been studied. These early efforts did not, however, lead to standards of design and construction for practical use. No standard reinforcing schemes were identified as most efficient. Other unexplored areas are composite material testing, quantification of the physical properties of the composite components, mechanical behavior, and standardizing test procedures, as also are those related to the effects of chemical degradation and environmental exposure as well as long-term performance of FRP composite systems. Cyclic loading is common in the case of bridge structures, but the effect of such loading on fatigue life of patch repairs is yet to be addressed. As a welcome first step, some ad hoc guidelines have appeared in recent times as ACI 440.2R-08 (Busel[6]) and NCHRP 655 (Zureick[7] et al.) reports for composite patch repair.

More recent researchers have tried to find answers to the unresolved issues. These specialized efforts are focusing on each element of a typical FRP composite system, namely, substrate material, surface preparation, adhesive, FRP fibrous material, and protective coating. Studies are being conducted on specific applications of FRP repair/strengthen schemes for structural members deficient in shear, flexural, torsional, and axial capacity. Of late, efforts have been directed to address issues like finding optimum reinforcing schemes, creating accurate response prediction models, and characterizing the long-term performance of FRP composites. With the introduction of newer FRP products, potential for new applications have been identified. The focus of the effort reported here is the development of a clear understanding of the physical phenomena of damaged precast beams bonded with readily available FRP composite patches in the local market, through laboratory tests, mechanistic modeling and finite element analysis.

TEST BEAM DETAILS

The three precast prestressed test beams were proportioned for a total limit load of 22.25 kips, keeping in view the available test facilities in the laboratory, appropriate weight of the test beams for ease of handling, feasibility of fabrication in laboratory conditions, and nature of tests to be undertaken. The details of the test beams are shown in Fig. 2. Two ½" dia. prestressing strands with ultimate tensile strength of 270 ksi are used. The top hanger bars

are of #3 size and stirrups are of #2 size. The average concrete strength at 28-days is 6.5 ksi. The beams were subjected to four-point loading, as shown in Fig. 3.

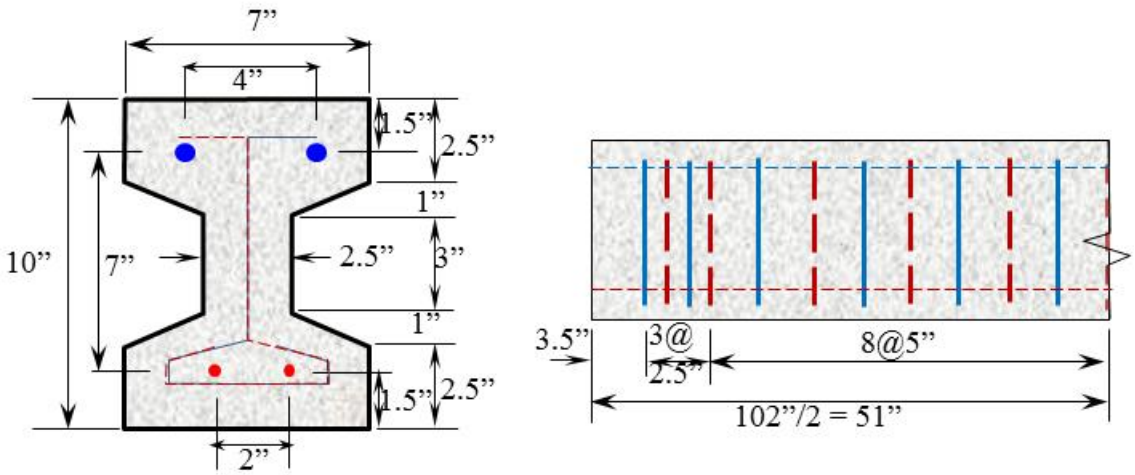

(a) Details of cross-section (b) Stirrups

Fig. 2 Prestressed concrete test beam

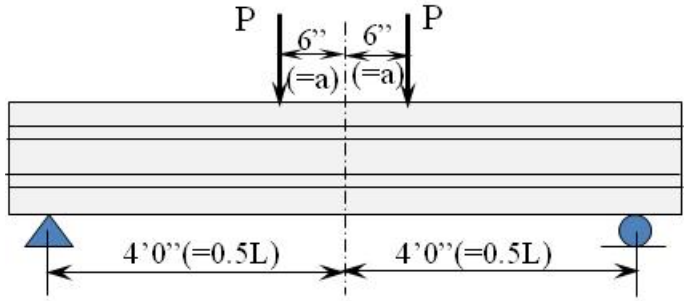

Fig. 3 Loading configuration

COMPOSITE PATCH MATERIAL

With no official standards, FRP materials are highly variable. The fiber and resinous matrix have distinct mechanical, thermal, and chemical properties. Manufacturers furnish limited technical information about FRP material and adhesive for applying to the substrate. The available information is not adequate for structural engineers to use in the design of FRP composite systems. Bank[8] explains the general lack of standardization of FRP composites and adhesives for civil engineering applications and provides pointers for the process to begin. Matters get worse due to the lack of standardized test procedures for determining the properties of composite materials and adhesives for civil engineering applications. Consequently, new experimental methods had to be developed in the context of this research to find adhesive properties, like equivalent spring stiffness constants in both tension and shear for use in the mechanistic and finite element models, adhesive tensile and shear modulus, adhesive tensile and shear capacity, and identification of the possible failure modes involving adhesives. In this study, the two distinct types of composite patch repair materials,

namely, SikaWrap Hex230 and Sika Carbodur were considered. Both these materials find application in civil engineering. For instance, SikaWrap Hex230 finds use in enhancing the earthquake resistance of round concrete columns in bridge piers by wrapping. Sika Carbodur is customized for bonded patch repair of concrete structures. This patch material is, however, quite expensive. The significant properties of these two materials are summarized in Table 1. A series of tests were undertaken with a universal testing machine and the resulting mechanical properties of the adhesives used are summarized in Table 2.

Table 1. Properties of composite patch material used

Designation	SikaWrap Hex230	Sika Carbodur
Carbon Fiber	Unidirectional-fabric	Unidirectional-Pultruded
Matrix	Sikadur 330	Sikadur 30
Adhesive	Sikadur 330	Sikadur 30
Application	Wet Process	Bonded
Curing	Heat/Pressure	Pressure
Factory thickness	0.01”	0.047”
Tensile strength	62.4 ksi	449 ksi
Tensile modulus	34,000 ksi	23,900 ksi
%Elongation	1.8	1.69

Table 2. Mechanical properties of adhesives

Designation	Sikadur 330	Sikadur 30
Shear modulus	0.44 ksi	16.00 ksi
Tensile modulus	0.77 ksi	23.89 ksi
Shear strength	0.32 ksi	1.59 ksi
Tensile strength	1.01 ksi	0.87 ksi
Tensile stiffness, k_v	7.73 kip/in^3	75.76 kip/in^3
Shear stiffness, k_h	8.77 kip/in^3	34.25 kip/in^3

PATCH DESIGN

Design of patch repair for prestressed concrete beams with flexure and shear cracks is discussed in the following. In order to ensure added safety, the nominal capacities of the section after repair, M_{nr} for moment and V_{nr} for shear, are ensured to be 10% more than the capacities, M_{nd} and V_{nd}, of as designed beams. So that

$$1.1M_{nd} = M_{nr} \geq M_u \quad (1)$$

$$1.1\boldsymbol{V_{nd}} = \boldsymbol{V_{nr}} \geq \boldsymbol{V_u} \quad (2)$$

In the prestrestressed concrete (PSC) section shown Fig. 4, apart from bottom steel strands of area A_{ps} and top reinforcing rods of area A_s', additional bottom reinforcing rods of area A_s is shown. Here, four flexural strength limit states can be identified, namely, (i) all steel elastic,

(ii) all steel plastic, (iii) top steel and strands elastic and bottom steel yielded, and (iv) top steel elastic and all bottom yielded. The flexural stresses and forces in the patch-repaired beam section are also shown in Fig. 4, with all steel yielded and concrete reaching the crushing strain. Summing the moment of the internal forces about the center of the composite patch yields the nominal moment capacity. Substitution of the expressions for F_c, F_s', F_{ps} and F_s into the moment capacity expression leads to the Eq. 3 for the neutral axis depth,

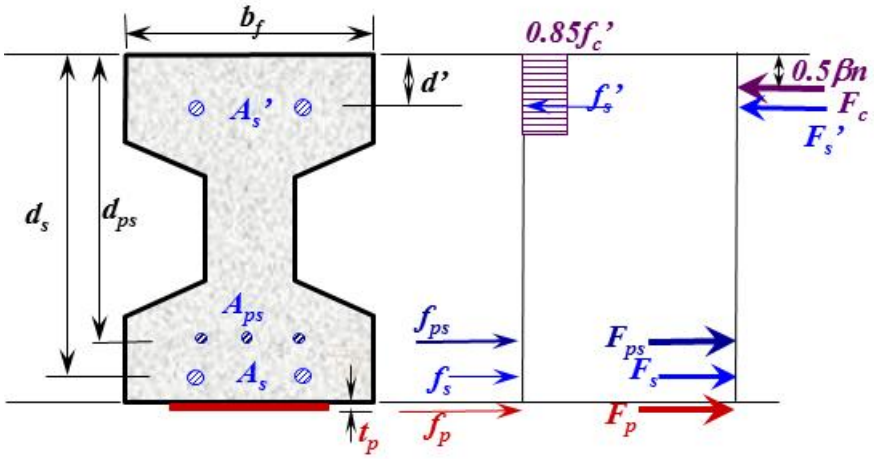

Fig. 4 Prestressed concrete beam (PSC) at flexural limit state

$$n = \frac{2d_p}{\beta}\left[1 - \sqrt{1 - \frac{M_{nr} + A_s f_y\left(d_p - d_s\right) - A_s' f_y\left(d_p - d'\right) - A_{ps} f_{ps}\left(d_p - d_{ps}\right)}{0.85 f_c' b d_p^2}}\right] \quad (3)$$

Eq. 3 is applicable when the rectangular stress block is confined within the rectangular part of the top flange. If the stress block extends beyond the rectangular part, the expression for F_c will be more involved. The notations used here follow the ACI Code. Using the value of n disclosed by Eq. 3, the strains can be checked and modified as needed. The design force for the patch can then be determined by satisfying the equilibrium of normal forces and the size of the patch can then be determined on the basis of specific allowable stress in the patch material.

Possible shear patch configurations are shown in Fig. 5, comprising of a pair of inclined side plates, a pair of vertical side plates, an inclined U-jacket and a vertical U-jacket. U-jackets are considered advantageous over side plates in the sense that, in the former case, the patch is prone to debonding above the crack only; whereas, in the latter case, the patch is prone to bond failure on both sides of the crack. Full wrapping of the beam is not possible because of the presence of the deck slab and also not desirable because of the possibility of explosive failure under overload.

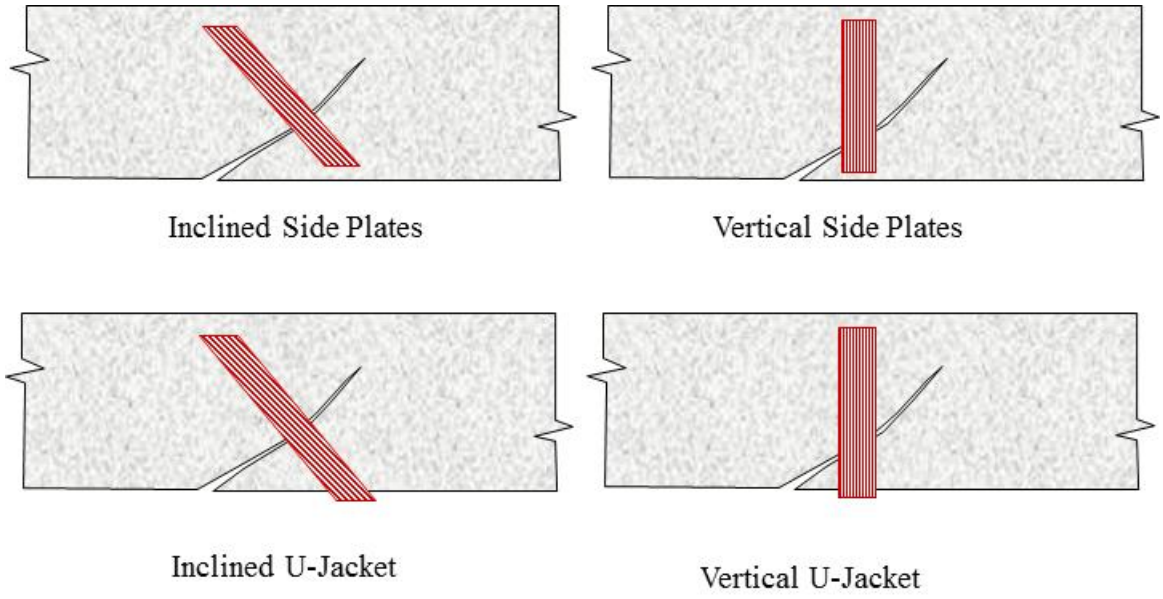

Fig. 5 Shear patch configurations

The shear capacity of the shear-patch shown Fig. 6 is given by Eq. 4 shown below.

$$V_p = V_n\big|_{\text{Required}} - (V_c + V_s) \tag{4}$$

with $V_c = \left(0.6\sqrt{f_c'} + 700\frac{V_u d}{M_u}\right) b_w d$ and $V_s = A_v f_y (\sin\alpha_s + \cos\alpha_s)\frac{d}{s}$

For some situations, the concrete resistance, V_c, may need to be ignored. The design force for each pair of patches is given by $F_p = V_p d / s(\sin\alpha_p + \cos\alpha_p)$. If only one pair of inclined patch strips is used, the design force for each patch will be $V_p / \sin\alpha_p$.

Once the design force in the patch material is determined, the theoretical width of a patch of given thickness, t_p, can be determined from

$$w_p = \frac{F_p}{0.9 f_{pu} t_p} \tag{5}$$

For practical reasons, the width provided will normally be more than the calculated value. An important aspect of the design is the need for providing adequate development length, to avoid the possibility of delamination. Assuming a triangular limiting bond stress distribution at the end of the patch with a peak adhesive stress f_a, the development length can be expressed as

$$L_{pd} = \frac{2 t_p f_p}{0.9 f_a} \tag{6}$$

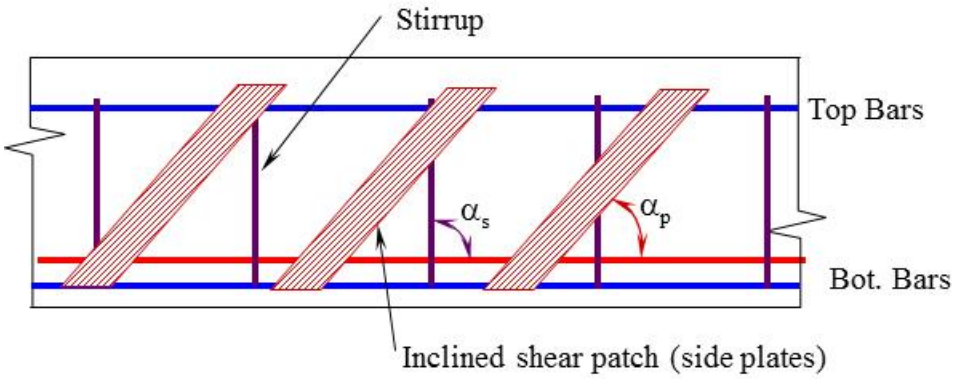

Fig. 6 Series of inclined patch strips in pairs

DAMAGE REPAIR

Two of the beams, designated as PSCB1 and PSCB2, were loaded as shown in Fig. 3, past the service load, to cause damage in the form of structural cracks. Beam PSCB1 developed shear cracks on one side and was loaded to 16.3 kips and PSCB2 developed flexural cracks near the center of span and was loaded to 24.3 kips. PSCB1 was subjected to shear patch repair using 8" wide Hexwrap U-jacket. The flexural patch repair of PSCB2 was done by bonding a 4"x18" Carbodur strip in the bottom flange, see Fig. 8. Further details of patch design are given in Table 3. Patch repair was followed by installation of sensors to measure the strains in the patches during load testing.

Table 3. Details of shear and flexure patches

Beam Designation	PSCB1	PSCB2
Patch Location	Web	Bottom flange
Patch Material	SikaWrap Hex230	Sika Carbodur
Strengthen for	Shear	Flexure
Patch shape	U-Jacket	Flat plate
Design Force, F_p	13.27 kips	6.37 kips
Required width	0.79"	0.37"
Width provided	8"	4"
Actual stress, f_p	55.1 ksi	33.91 ksi
Required Length	33"	16.72"
Length provided	33"	18"
Slope, α_p	90^o	NA

The patch repair of beams PSCB1 and PSCB2 are shown in Fig. 8. Fig. 8(a) shows the bonded Hexwrap U-jacket covering the shear cracks in PSCB1. Fig. 8(b) shows the bonded

Carbodur plate spanning the flexure cracks in the bottom flange.

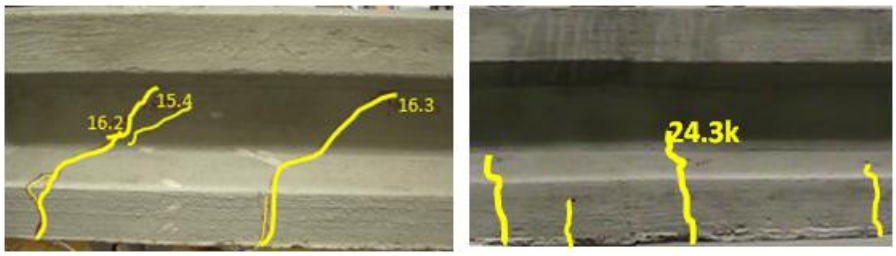

(a) Shear crack in PSCB1 near right support (b) Flexure cracks in PSCB2 near midspan

Fig. 7 Cracks in damaged beams before repair

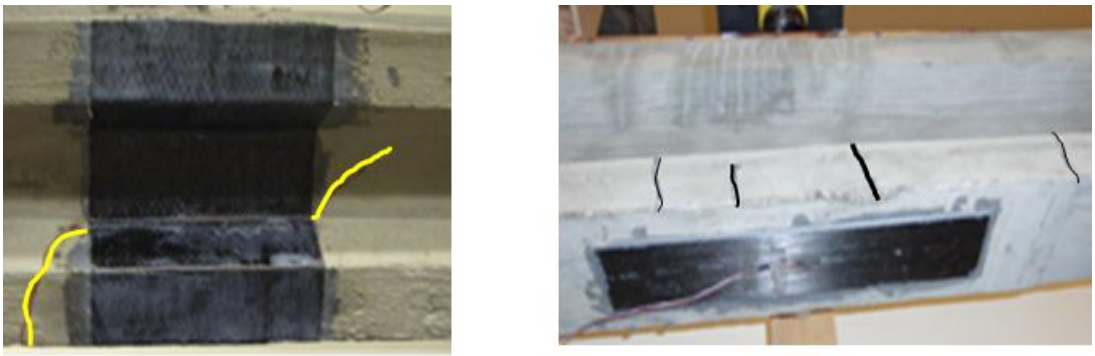

(a) Hexwrap U-Jacket patch (b) Carbodur patch in bottom

Fig. 8 Patch repaired beams PSCB1 and PSCB2

Fig. 9 Load testing of PSCB2 in progress

TESTING OF REPAIRED BEAMS

The patch repairs were first instrumented with strain gages, as can be seen in Fig. 8(b), and then the beams were subjected to the same four-point loading setup, shown in Fig. 9, similar to what was done to cause damage to the beams before undertaking any repair. The load was applied at ASTM specified loading rates for concrete beams. Loading was continued until failure. Data on load vs. deflection as well as load vs. strain were recorded. In the case of PSCB1, the failure was again in shear, initiated by the elongation of existing cracks and creation of new shear cracks, Fig. 10(a). This was followed by progressive cracking of the patch normal to the axis of the carbon fibers in the U-jacket accompanied by debonding, especially near the bottom flange, Fig. 10(b). In this case, the failure load hardly exceeded the failure load without patch. However, the beam continued to support the maximum load

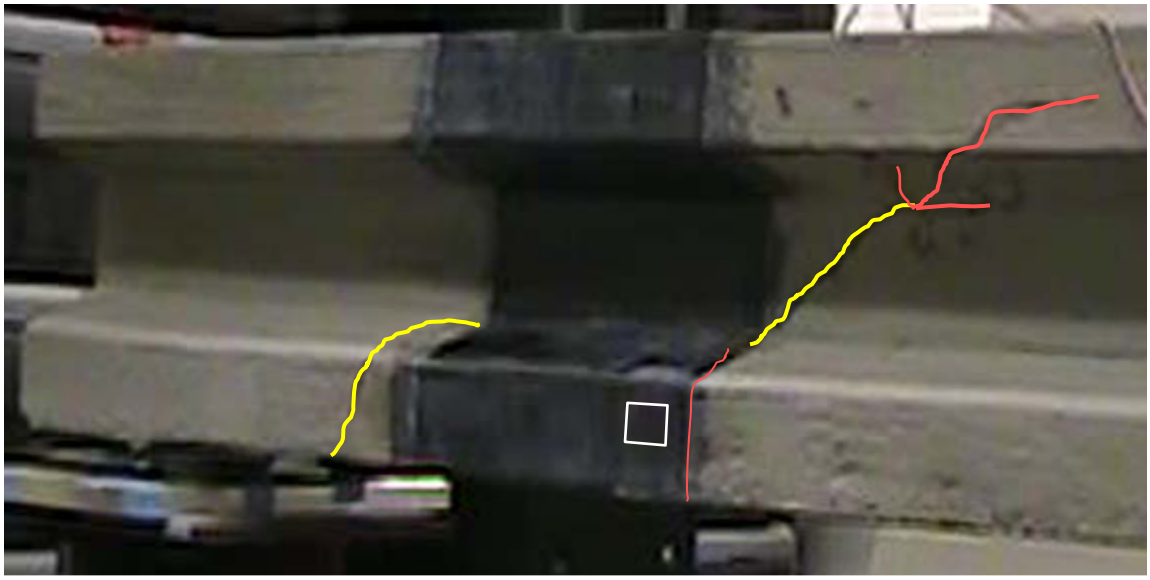

(a) Cracking of PSCB1 at a load of 16 kips

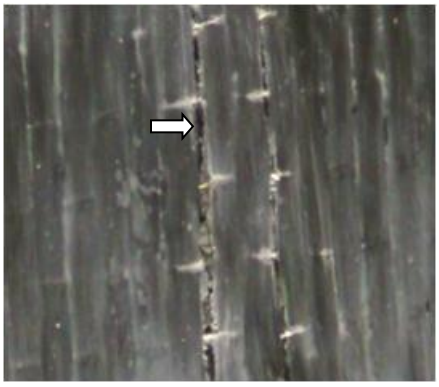

(b) Cracking of U-jacket in the boxed area shown above

Fig. 10

reached under increasing deformation, showing significant ductility. No flexural cracking in the maximum moment region was noticed. The load vs. deflection experimental curve for virgin PSCB1 is shown in Fig. 14. In Fig. 15 is shown the variation of experimental normal strain in the top of beam with the applied load. In the case of PSCB2, the final failure was also in shear taking place suddenly at a load of 30.5kips. The flexure patch repair seemed to do its job well. The shear failure of PSCB2, occurring just at one support, is shown in Fig. 11(b). The plots of Figs. 16 to 18 give the variation of experimental central deflection, top normal strain and maximum patch strain for flexural patch repaired PSCB2.

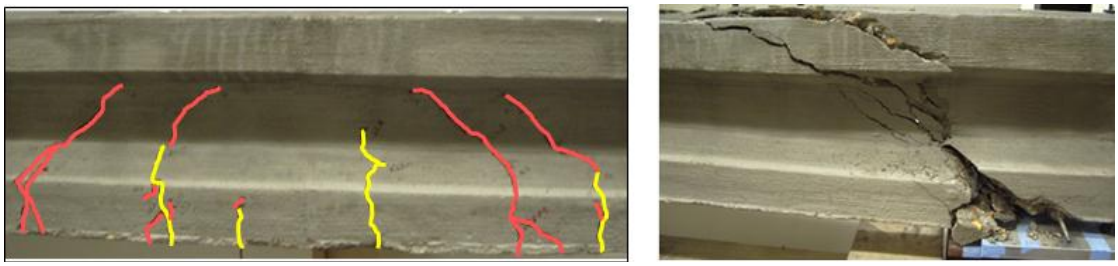

(a) Flexural cracks at failure load (b) Failure caused by shear cracks near one support

Fig. 11 Failure patterns of PSCB2 after repair

MECHANISTIC MODEL DEVELOPMENT

As a simpler alternative to finite element analysis, a scheme for reasonably accurate analysis of bonded patch repair of bottom flange of the beam was developed based on time tested principles of mechanics. The analysis is valid up to the limit state. A schematic view of the beam is shown in Fig. 12(a). Fig. 12(b) shows normal and shear spring model to represent the normal and tangential resistance of the adhesive layer. Tests were conducted to determine the equivalent spring constants for the adhesive, as shown in Table 2. One common assumption made in the analysis is that the plane sections in the beam as well as patch remain so, allowing relative deformation between the two. The effect of material nonlinearity in concrete is allowed for indirectly by modifying the stiffness with the progression of damage. No delamination of patch is allowed. The total potential energy of the beam can then be expressed as Eq. 7.

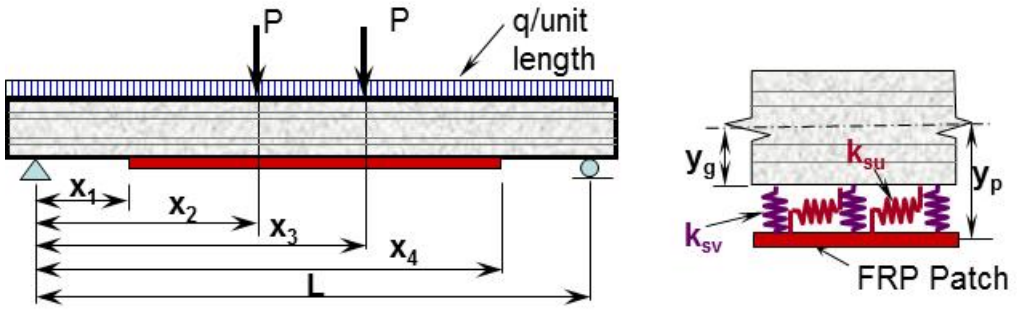

(a) (b)

Fig. 12 Simply supported beam with flexural patch repair in bottom

$$\Pi = \frac{1}{2}\int_0^{x_1}(EI)_g\left(\frac{d^2v_g}{dx^2}\right)^2 dx + \frac{1}{2}\int_{x_1}^{x_4}(EI)_g\left(\frac{d^2v_g}{dx^2}\right)^2 dx + \frac{1}{2}\int_{x_4}^{L}(EI)_g\left(\frac{d^2v_g}{dx^2}\right)^2 dx +$$
$$\frac{1}{2}\int_{x_1}^{x_4}(EI)_p\left(\frac{d^2v_p}{dx^2}\right)^2 dx + \frac{1}{2}\int_{x_1}^{x_4}(EA)_p y_p^2\left(\frac{d^2v_p}{dx^2}\right)^2 dx + \frac{1}{2}\int_{x_1}^{x_4}\left(k_{sv}\delta_{sv}^2 + k_{su}\delta_{su}^2\right)dx -$$
$$\int_0^L qv_g dx - P\left[v_g(x_2) + v_g(x_3)\right] \qquad (7)$$

In this expression, v_g and v_p are vertical displacements of the beam and patch at any point, $(EI)_g$ and $(EI)_p$ are flexural rigidities of the beam and the patch at any point, $(EA)_p$ is the axial rigidity of the patch, and y_p is defined in Fig. 12. Also, $\delta_{sv} = v_g - v_p$, and $\delta_{su} = y_g\frac{dv_g}{dx} - \frac{t_p}{2}\frac{dv_p}{dx}$ are the extensions of the equivalent vertical and horizontal springs representing the stiffness of the adhesive at the interface of patch and beam bottom. In solving the problem, the unknown deflections, v_b and v_p, will be represented by the following Fourier series with unknown coefficients.

$$v_b = \sum_{i=1,3,5,\ldots}^{n} C_i \sin\left(\frac{i\pi x}{L}\right) \qquad (8)$$

$$v_p = \sum_{i=1,3,5,\ldots}^{n} C_i \sin\left(\frac{i\pi x}{L}\right) + C_o\bar{x}\left(L_p - \bar{x}\right) \qquad (9)$$

where, $\bar{x} = x - x_1$.

On substituting the expressions for v_b and v_p in Eq. (8) and Eq. (9) into Eq. (7), there will be $(n+1)$ unknowns coefficients, C_i, $i = 0,1,\ldots,n$. To determine these coefficients, the

stationary condition $\delta\Pi = 0$ can be applied, so that the following set of $(n+1)$ equations will be obtained.

$$\frac{\partial \Pi}{\partial C_i} = 0, \quad i = 0,1,3,...n \tag{10}$$

These equations can now be solved for the $(n+1)$ C_i values. The deflections, strains and stresses at any point in the parent beam and the composite patch as well as the adhesive can then be calculated. The accuracy of the values will depend upon the number of terms, n, used. Usually, three to five terms will give adequate accuracy. It may, however, be added that the length of patch, $L_p = (x_4 - x_1)$, is theoretical length and the patch should be continued beyond the theoretical cut-off point to develop the stresses at points x_1 and x_4.

As the load is increased on the patch-repaired beam and the limit load is approached, the beam will undergo flexural cracking and eventually fail by crushing of concrete above the neutral axis. Therefore, the $(EI)_g$ value for the beam will change as cracking progresses. In this situation beam flexural rigidity at any section will depend at the load level and also on the location of the section. Noting that $(EI)_g$ can be taken as moment divided by curvature, the moment vs. curvature relationships for the beam were based on the assumption that the compressive stress distribution can be represented by Hognestad et al.[9] stress vs. strain relationship for concrete. Tension stiffening action in concrete is represented by Renata et al.[15] model.

The result of mechanistic model for virgin PSCB1 is shown in Fig. 14, showing somewhat stiffer response than experimental result. This may be attributed to the assumption of perfect interfacial bond between concrete and strands/rebars. In the case of patch-repaired beam PSCB2, the Fig. 16 plot of load vs. central deflection based on mechanistic model shows good agreement with experimental data in the early phases of loading, but appears to be stiffer at higher loads, further confirming the effect of perfect bond assumption in the mechanistic model. In Fig. 17, however, the top strain values at midspan show reasonable agreement with experiments.

FINITE ELEMENT ANALYSIS

An important milestone of this effort was that it was for the first time (Yapar et al.[10]) a prestressed concrete beam was modeled with Abaqus, exactly the way pre-tensioned strands transfer the prestress to concrete. In other words, the model precisely followed the steps of stress inducement actually done in practice. Existing finite element models are crude and do not accurately represent the state of stress at various stages of loading. Even the very recent models seem to be half-hearted attempts, including the recent papers by Ayoub et al.[11], Arab et al.[12], and Okumus, et al[13]. Surprisingly, of these, the 2012 paper seems to be most off the track.

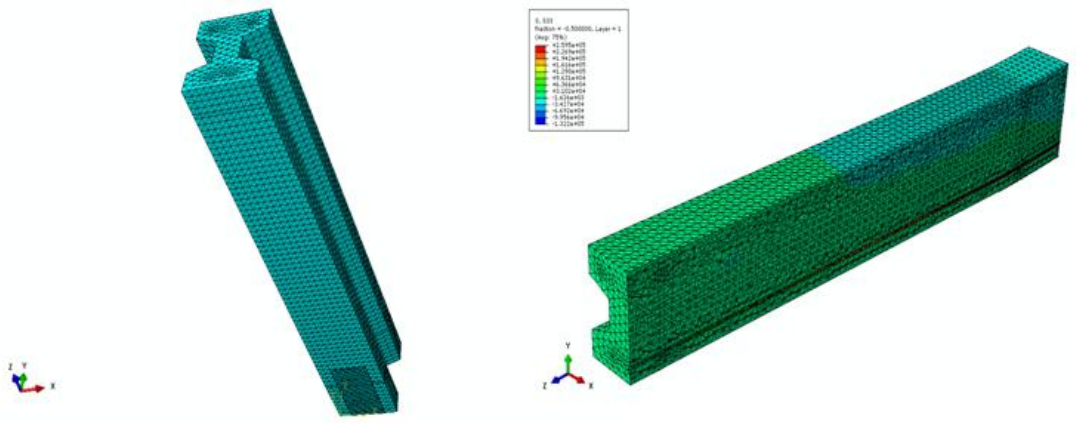

(a) Finite element model for half beam (b) Longitudinal stress (S33) contours
Fig. 13 Finite element modeling of flexural PSC beam with bottom patch repair

In the model developed for the present study, the properties of concrete, namely, tensile, compressive and bond behaviors were properly characterized. The model also included tension stiffening action allowing for progressive micro-cracking in concrete with a stiffness which is higher than the one based on no tension resistance in concrete. The concrete behavior is represented by using the concrete damage plasticity (CDP) model. This model assumes two main failure modes of concrete which are tensile cracking and compressive crushing (Hibbitt et al.[14]). In the CDP model, the compression data of the concrete was input as a function of compressive stress versus inelastic strain. Behaviors of reinforcing steel and prestressing strand were defined as elastic-perfectly plastic. The yield strength of unstressed steel was taken as 60 ksi. The bond between the reinforcement and the concrete was assumed as cohesive with stiffness of 5.72 k/in. The yield strength of strand was taken as 243 ksi. The ultimate compressive strength of concrete was taken as the usual compressive strength of concrete (f_c') which was defined as 6.5 ksi. The crushing strain corresponding to the ultimate compressive strength of concrete was defined as 0.003. The ultimate strain at which the compressive stress reaches zero was taken as 0.005. For the sake of computational efficiency, the symmetry of the beam about its center line was taken advantage of by considering only one-half of the beam and applying appropriate boundary conditions at the line of symmetry. The finite element model shown in Fig. 13(a) comprises of 62,636 C3D4 elements, and in the Carbodur patch there are 420 C3D8R elements. The stirrups did not form a closed loop, so were ignored in the model. Fig. 13(b) shows the normal stress contours in the longitudinal sectional view of the beam.

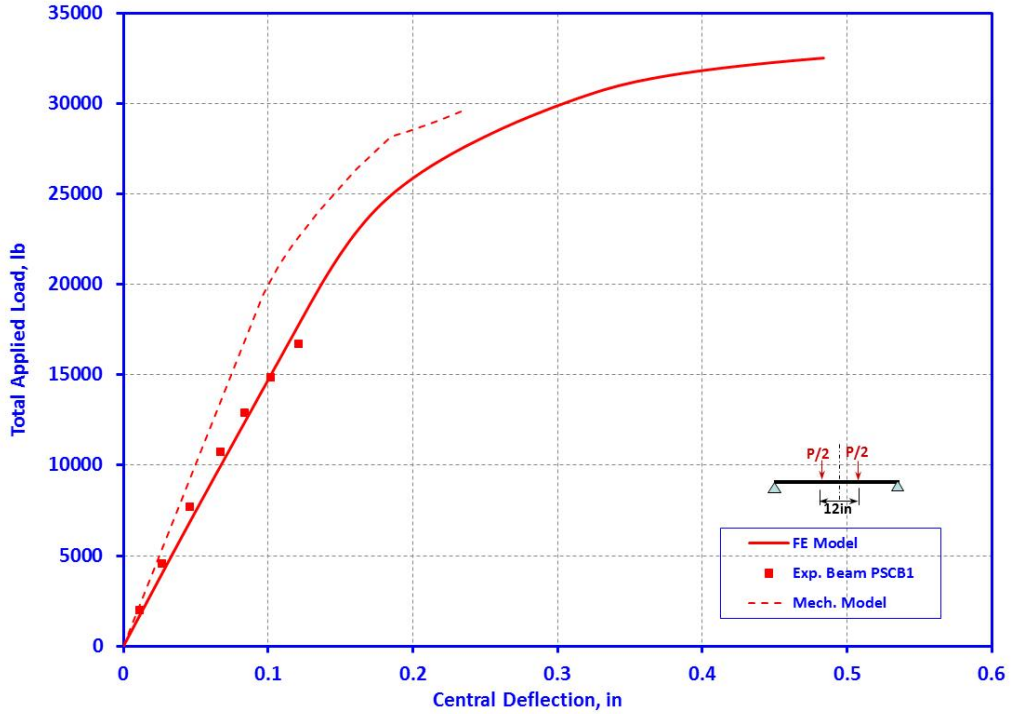

Fig. 14 Variation of deflection with applied load for virgin PSCB1

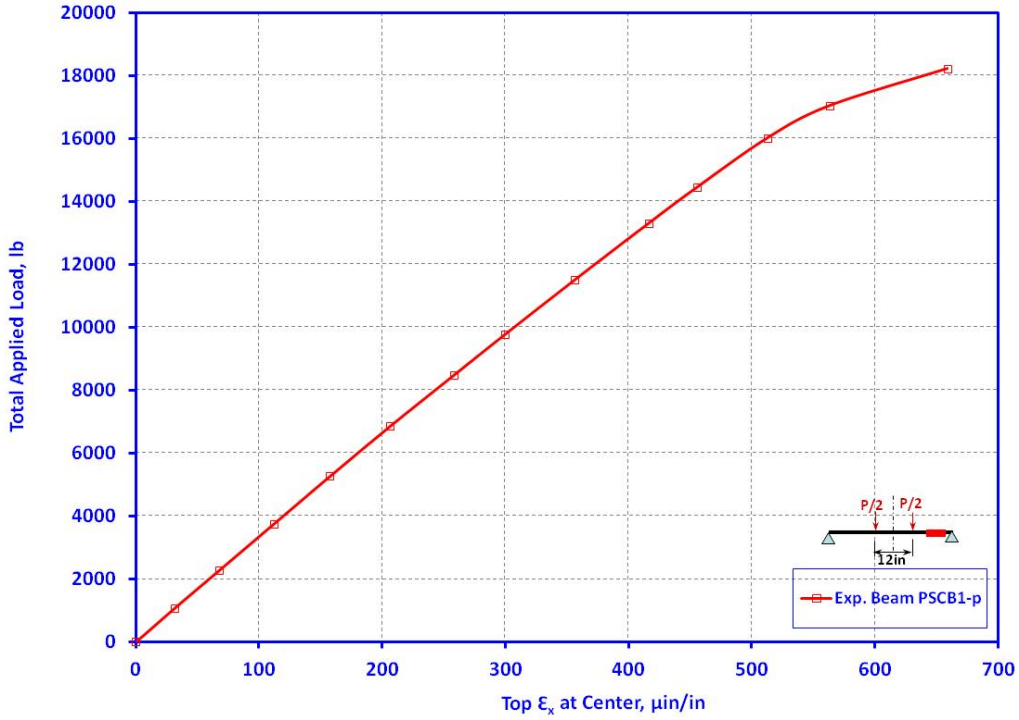

Fig. 15 Variation of maximum concrete strain with applied load for PSCB1

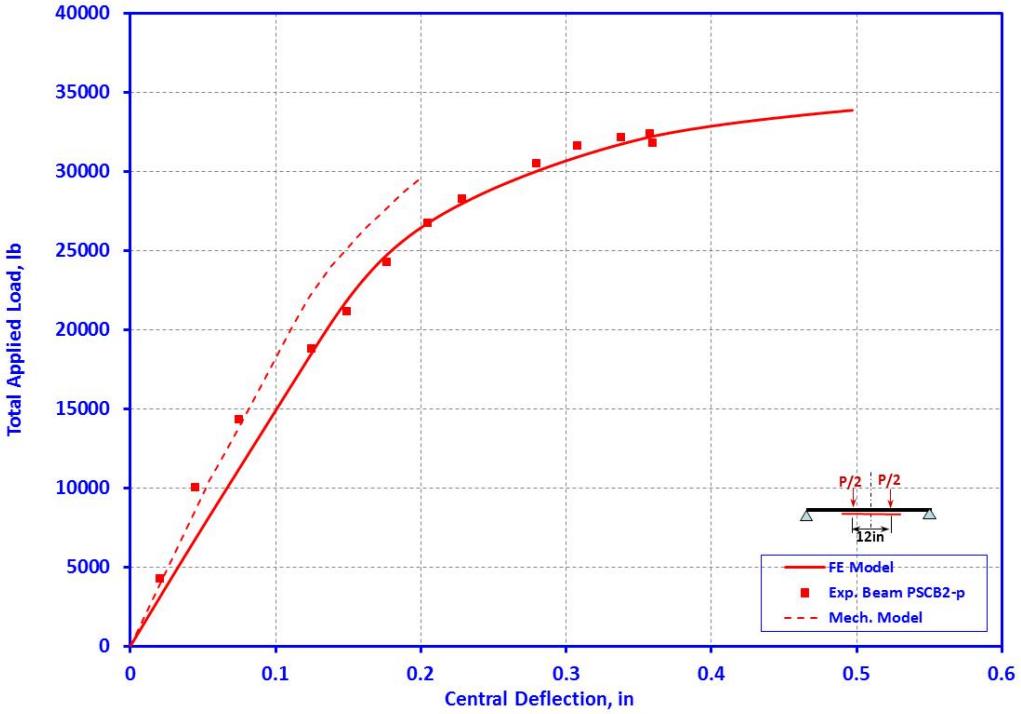

Fig. 16 Variation of central deflection with applied load for PSCB2

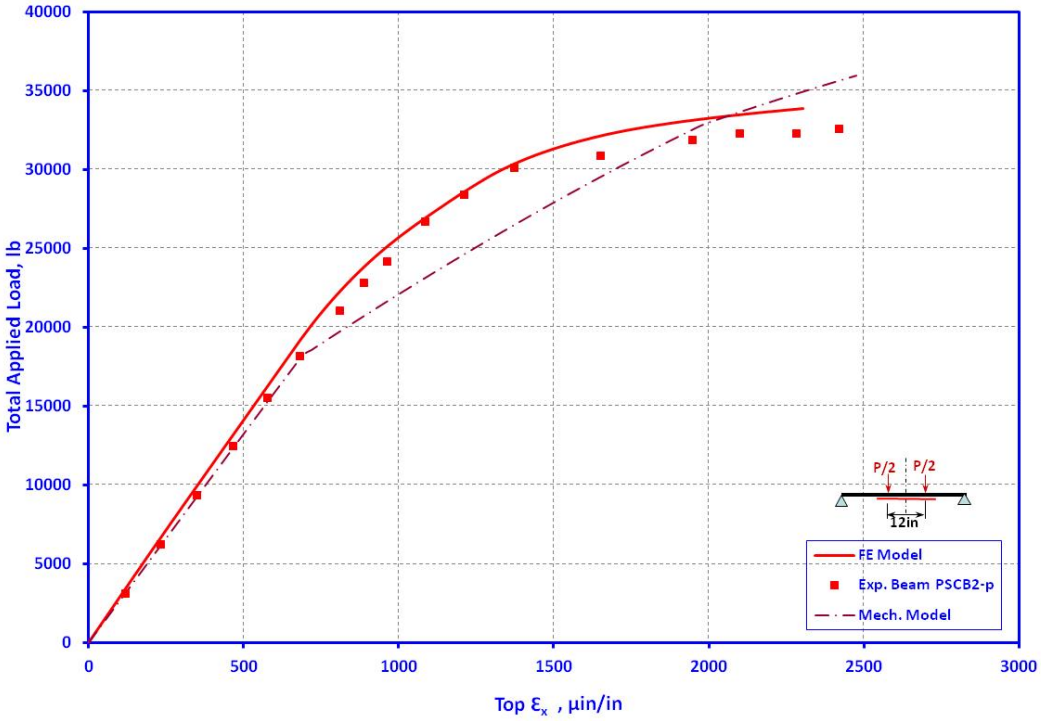

Fig. 17 Variation of maximum top strain with applied load for PSCB2

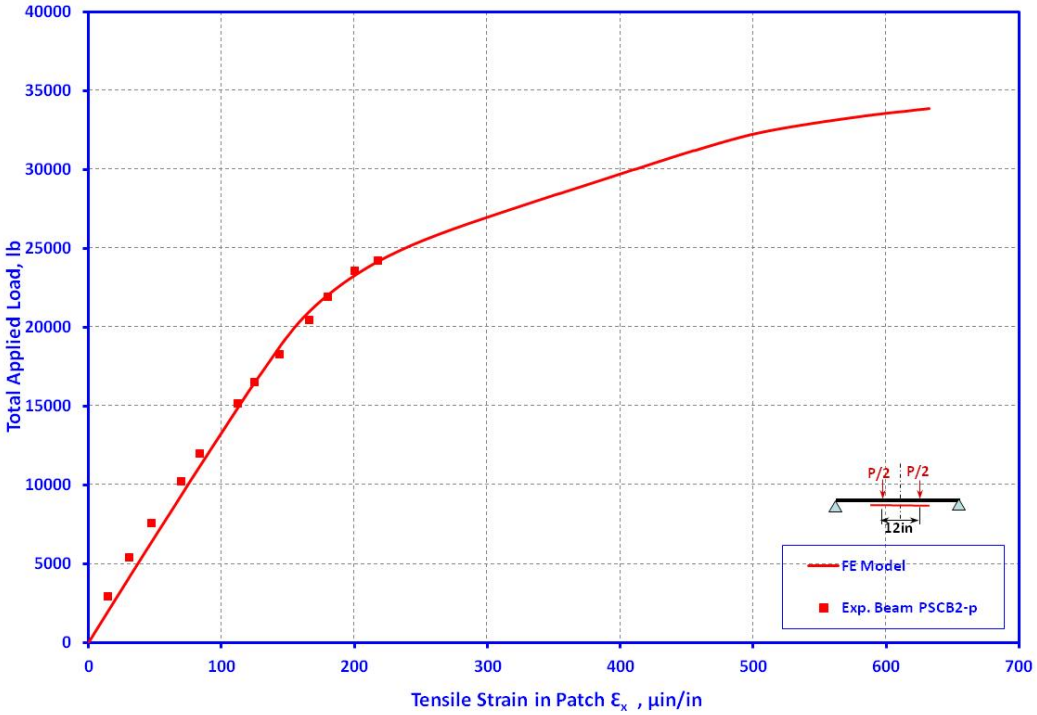

Fig. 18 Variation of maximum patch strain with applied load for PSCB2

The finite element results are for virgin PSCB1 (applicable to PSCB2 as well) and patch-repaired PSCB2 are shown in Figs. 14, 16 thru 18. In general, the results show excellent agreement with experimental data. However, the mechanistic model results in Fig. 14 appear to represent somewhat stiffer behavior, but those in Fig. 17 show better agreement with respect to finite element results.

SUMMARY & CONCLUSIONS

The issues related to FRP patch repair of PSC beams with localized damage were discussed and the need for standardization of manufacture, design and installation of such repair was emphasized. Apart from simple design formulas, a mechanistic model for flexural patch repaired prestressed I-beams were presented. Experimental studies on test prestressed concrete beams with flexural and shear patch repair were also presented. Accurate finite element models for the beams were considered and the resulting response predictions were compared with experimental data and mechanistic model results.

FRP patch repair of precast prestressed concrete bridge beams can be an effective means to extend the useful life provided great care is taken in pursuing the repair work. Patch repair can be designed easily with the formulas developed for the purpose. The proposed mechanistic model can be used for response prediction of the repaired beam after some adjustments to account for interfacial bond behavior between strand and concrete. The

proposed finite element model gives highly accurate prediction of the behavior of a precast prestressed beam with and without patch repair and can be extended to beams of any span.

ACKNOWLEDGEMENT

Tennessee Department of Transportation funded the major part of this research effort and Adrian A. Bennett assisted in designing the test beam as per AASHTO standards. Material help from Sika Corporation for composite patch material and Concrete Products, Inc. for concrete raw materials is acknowledged.

REFERENCES

1. Schust, S.M. (2008), “$140 Billion Price Tag to Repair and Modernize America's Bridges,” AASHTO Press Release, July 28, Web.

2. Harries, K.A., Kasan, J., Aktas, C.J. (2009), “Repair methods for prestressed girders,” Report No. FHWA-PA-2009-008-PIT 006, Penn DOT, June.

3. Basu, P.K., Yapar, O., and McNutt, J.N., “Life extension of bridge superstructure components with composite patch repair,” to appear in Proc. of International Conference on Structural Faults and Repair, July 2012, Edinburgh, UK.

4. Ahn, Jae. S., and Basu, Prodyot K. (2011), “Locally refined p-FEM modeling of patch repaired plates,” Composite Structures, Vol. 89, No. 4, pp. 524-535.

5. Meier, U. (1995), “Strengthening of Structures Using Carbon Fiber/Epoxy Composites,” Construction and Building Materials, 9.6, 341-51.

6. Busel, John P. (2008), Guide for the Design and Construction of Externally Bonded FRP Systems for Strengthening Concrete Structures. ACI 440.2R-08. Michigan: American Concrete Institute.

7. Zureick, Abdul-Hamid, Bruce R. Ellingwood, Andrzej S. Nowak, Dennis R. Mertz, and Thanasis C. Triantafillou. (2010), “Recommended Guide Specification for the Design of Externally Bonded FRP Systems for Repair and Strengthening of Concrete Bridge Elements,” Rep. No. 655. Washington D.C.: National Cooperative Highway Research Program.

8. Bank, L. (2003) "A Model Specification for FRP Composites for Civil Engineering Structures." Construction and Building Materials, 17, 6-7, 405-437.

9. Hognestad E, Hanson NW, McHenry D. (1955) “Concrete stress distribution in ultimate strength design,” ACI Journal, Proc. 1955, 52, 12, 455-479.

10. Yapar, O., Nordendale, N.A., and Basu, P.K., “Accurate finite element modeling of pre-tensioned prestressed concrete beams,” in preparation.

11. Ayoub, A., and Filippou, F.C. (2010) “Finite-element model for pre-tensioned prestressed concrete girders,” J. Structural Engineering, Vol. 36, No. 4, April, 401-409.

12. Arab, A.A., Badie, S.S., and Manzari, M.T. (2011) “A methodological approach for finite element modeling of pre-tensioned concrete members at the release of pretensioning,” Engineering Structures, Vol. 33, 1918-1929

13. Okumus, P., Oliva, M.G., and Becker, S. (2012) “Nonlinear finite element modeling of cracking at ends of pretensioned bridge girders,” Engineering Structures, 40, 267-275.

14. Hibbitt, Karlsson, and Sorensen, Inc. (2000), “ABAQUS theory manual, user Manual and example manual,” Version 6.7. Providence, RI.

15. Renata S.B. Stramandinoli, Henriette L. La Rovere. (2008) “An efficient tension-stiffening model for nonlinear analysis of reinforced concrete members”, Engineering Structures, 30, 2069–2080.